NAVAL POSTGRADUATE SCHOOL
Monterey, California

THESIS

A NUMERICAL STUDY OF RAIN-INDUCED SURFACE GRAVITY WAVE ATTENUATION

by

David W. Howell

June 1989

Thesis Advisor: Jeffrey A. Nystuen

Approved for public release; distribution is unlimited.

Unclassified

security classification of this page

REPORT DOCUMENTATION PAGE

1a Report Security Classification Unclassified			1b Restrictive Markings
2a Security Classification Authority			3 Distribution Availability of Report Approved for public release: distribution is unlimited.
2b Declassification Downgrading Schedule			
4 Performing Organization Report Number(s)			5 Monitoring Organization Report Number(s)
6a Name of Performing Organization Naval Postgraduate School	6b Office Symbol *(if applicable)* 35		7a Name of Monitoring Organization Naval Postgraduate School
6c Address *(city, state, and ZIP code)* Monterey, CA 93943-5000			7b Address *(city, state, and ZIP code)* Monterey, CA 93943-5000
8a Name of Funding Sponsoring Organization	8b Office Symbol *(if applicable)*		9 Procurement Instrument Identification Number
8c Address *(city, state, and ZIP code)*			10 Source of Funding Numbers
		Program Element No	Project No / Task No / Work Unit Accession No

11 Title *(include security classification)* A NUMERICAL STUDY OF RAIN-INDUCED SURFACE GRAVITY WAVE ATTENUATION

12 Persona. Author(s) David W. Howell

13a Type of Report	13b Time Covered	14 Date of Report *(year, month, day)*	15 Page Count
Master's Thesis	From To	June 1989	38

16 Supplementary Notation The views expressed in this thesis are those of the author and do not reflect the official policy or position of the Department of Defense or the U.S. Government.

17 Cosati Codes			18 Subject Terms *(continue on reverse if necessary and identify by block number)*
Field	Group	Subgroup	Ocean Waves, Attenuation, Vortex Rings

19 Abstract *(continue on reverse if necessary and identify by block number)*

Strong rain-induced mixing in a thin surface layer is numerically shown to greatly increase surface gravity wave attenuation. This case study uses a single wavelength (2.8 m) together with two mixed layer depths (10 and 20 cm). The rain-induced mixing is simulated by varying kinematic viscosity within the mixed layer from 10^{-6} to 10^{-3} $m^2 s^{-1}$, molecular to strong turbulent mixing, respectively. The results indicate that surface gravity wave attenuation in the presence of a thin rain-induced mixed layer can increase by a factor of up to 6000 times the attenuation rate due to molecular viscosity alone. This indicates that rain need only mix the top 10-20 cm surface layer to effectively dampen short surface gravity waves.

20 Distribution Availability of Abstract	21 Abstract Security Classification	
☒ unclassified unlimited ☐ same as report ☐ DTIC users	Unclassified	
22a Name of Responsible Individual Jeff Nystuen	22b Telephone *(include Area code)* (408) 646-2917 2552	22c Office Symbol 68NY

DD FORM 1473,84 MAR 83 APR edition may be used until exhausted
All other editions are obsolete

security classification of this page

Unclassified

Approved for public release; distribution is unlimited.

A Numerical Study of Rain-Induced
Surface Gravity Wave Attenuation

by

David W. Howell
Lieutenant, United States Navy
B.S., Texas A&M University, 1979

Submitted in partial fulfillment of the
requirements for the degree of

MASTER OF SCIENCE IN METEOROLOGY AND PHYSICAL OCEANOGRAPHY

from the

NAVAL POSTGRADUATE SCHOOL
June 1989

Author: David W. Howell
David W. Howell

Approved by: Jeffrey A. Nystuen
Jeffrey A. Nystuen, Thesis Advisor

Roland W. Garwood
Roland W. Garwood, Second Reader

Curtis A. Collins
Curtis A. Collins, Chairman,
Department of Oceanography

Gordon E. Schacher
Gordon E. Schacher,
Dean of Science and Engineering

TABLE OF CONTENTS

LIST OF TABLES

LIST OF FIGURES

ACKNOWLEDGEMENTS

I would like to thank Professor Jeffrey Nystuen and Professor Roland Garwood for their unending support and answers to my many questions. A special thanks also goes to my wife, Anna, for her support, guidance, skillful typing and patience in the writing of this manuscript.

I. ABSTRACT

Strong rain-induced mixing in a thin surface layer is numerically shown to greatly increase surface gravity wave attenuation. This case study uses a single wavelength (2.8 m) together with two mixed layer depths (10 and 20 cm). The rain-induced mixing is simulated by varying kinematic viscosity within the mixed layer from 10^{-6} to $10^{-2}\ m^2\ s^{-1}$, molecular to strong turbulent mixing, respectively. The results indicate that surface gravity wave attenuation in the presence of a thin rain-induced mixed layer can increase by a factor of up to 6000 times the attenuation rate due to molecular viscosity alone. This indicates that rain need only mix the top 10-20 cm surface layer to effectively dampen short surface gravity waves.

II. INTRODUCTION

For centuries sailors and casual observers living along the coast have observed that ocean waves are dampened, and the sea becomes flat during rain. This dampening is evident especially during rain events when winds are light or calm. This dampening must be a result of energy transfer from a raindrop that strikes the ocean surface. The raindrop impact may generate capillary waves, subsurface turbulent mixing, and sound or heat. Only subsurface turbulent mixing is likely to interact with surface gravity waves. This process, first suggested by Reynolds (1900), takes the form of vortex rings which propagate downward, mixing the water in a near surface layer as the rings disintegrate; thus enabling the vortex rings to effectively increase the turbulent mixing in a thin layer near the surface of the water.

Manton (1973) used an analytical approach based on Reynolds' idea, to argue that rain-induced mixing will cause surface gravity wave attenuation. Manton assumed a constant eddy viscosity throughout the water column to solve his governing momentum equations. The assumption of no depth dependence of the mixing seems unrealistic. The scope of this study is to examine, by numerical methods, the effects of increased turbulent mixing due to rain in a thin surface layer. It is hypothesized that by increasing the turbulent mixing in a thin surface layer, significant attenuation of a surface gravity wave will result. This study focuses on waves having a wavelength of 2.8 m and amplitudes of 3 and 6 cm. Eddy viscosity is varied from 10^{-6} to $10^{-2}\, m^2\, s^{-1}$. The mixed layer depth is either 10 cm or 20 cm. The rate of kinetic energy change at each time step was calculated and used to determine the rate of wave attenuation. The use of a numerical calculation allowed viscosity to be varied with depth. Alternatively, Manton employed

a velocity potential solution; however, this precluded solving for the rotational flows occurring here.

A. SIGNIFICANCE

The dampening of waves by rain can influence satellite remote sensing observations at the sea surface, in addition to changing the characteristics of the water column. Satellite borne scatterometers and Synthetic-Aperture Radars (SAR) measure microwave energy backscattered to space from the ocean's surface. Scatterometers are able to determine wind speeds based on the energy backscattered from the sea surface by short surface gravity waves (approximately 30 cm). If these waves are attenuated by rain, scatterometer-derived winds will be in error for areas under a rain event, giving the impression that there are light winds present when in fact greater winds may be present.

Fu and Holt (1982) noticed that squall storm lines were easily detected in SAR images. They found that down draft and rain areas were delineated by changes in image brightness. The image was brighter in the outflow area due to a rough sea surface. A smooth dark image caused by the absence of backscattered energy suggested that in areas of rain the capillary and short gravity waves had been dampened.

Rain also influences the water column. Livezey (1988) found that rain events could cause changes to the seasonal mixed layer depth indirectly effecting heat loss to the atmosphere. Using a total kinetic energy budget model, Garwood (1989) demonstrated that a rain-generated mixed layer would form in a stratified water column. A 200 cm mixed layer depth (MLD) was produced when turbulent kinetic energy (TKE) of a rain event was injected into the upper layer of the ocean, see Fig. 1. Within 1000 seconds the MLD is seen to be approaching steady state. A continued deepening of the MLD will occur, but at a much slower rate until equilibrium has been reached. The results are tentative, but do suggest that rain has a possible role in ocean mixed layer dynamics.

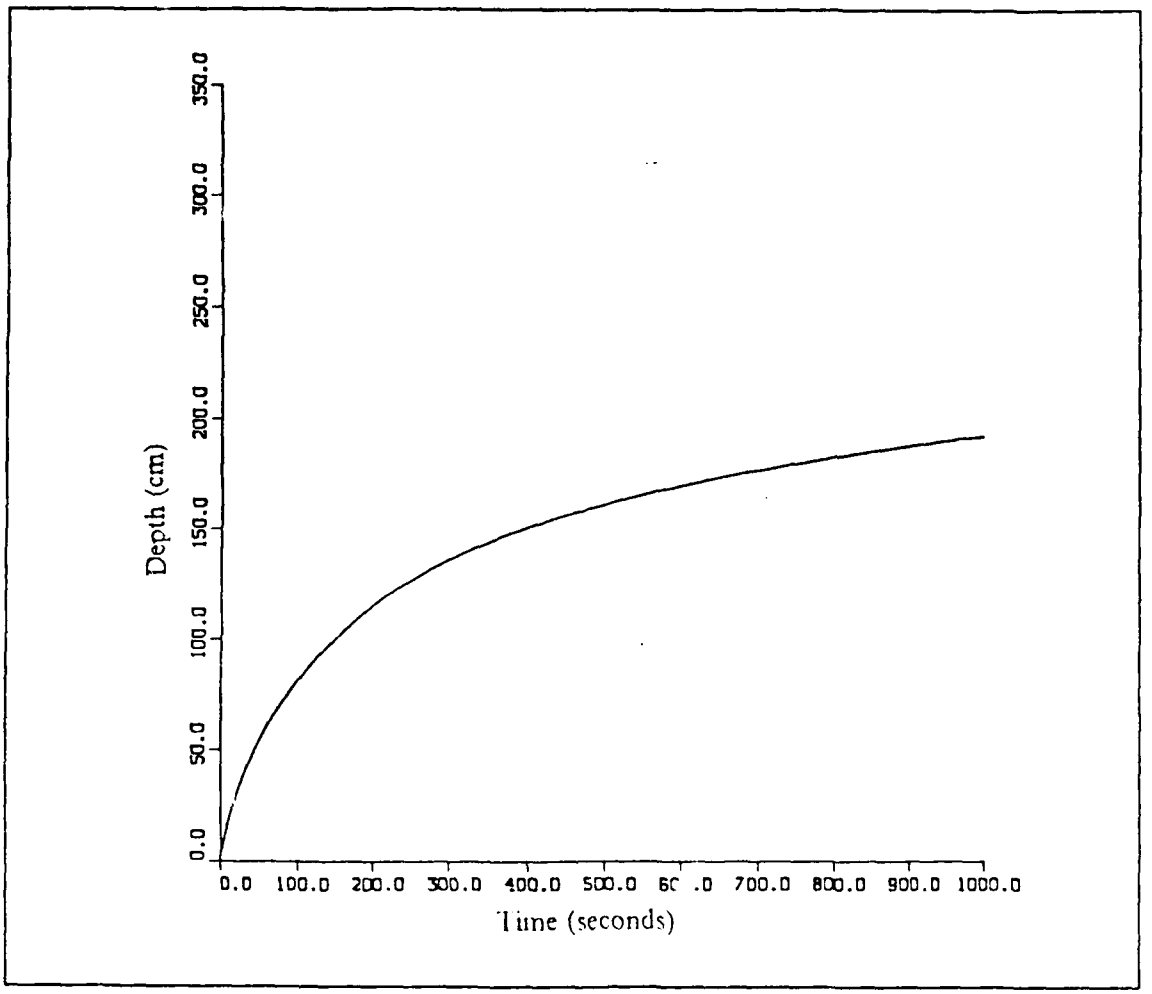

Figure 1. Mixed layer depth prediction: A 200 cm mixed layer has formed by rain-injected TKE.

When a raindrop strikes a fluid surface there are other interesting effects. One effect is a roughening of the sea surface from depression cusps that break the smoothness of the sea surface. In conjunction with the wind, the roughened surface caused an increase in the surface stress. This stress increase augments the transfer of energy into the water column. Caldwell and Elliott (1970) found that a rain rate of several centimeters per hour in light winds could produce stresses comparable in magnitude to the wind stress

for winds as high as 10-20 $m\,s^{-1}$ without rain. A heavy rain can also produce bubble clouds, a layer of bubbles beneath the wave surface, similar to those produced by breaking waves. Thorpe (1984) used these bubble clouds to examine the effects of Langmuir circulation by following their progress through the water column. In his study he found that the Langmuir circulation increased the flux of gases down into the water column. Rain is thus able to effect directly the surface roughness and stress, and to effect indirectly the flux of gas into water column.

B. LITERATURE REVIEW

1. Surface Effects Due to Rain

Reynolds (1900) observed water drops falling into a glass vessel and he postulated the first explanation for wave attenuation. From his study of vortex rings, he believed that the " knocking down " of waves resulted from mixing of subsurface water by vortex rings formed by the raindrops hitting the surface. As the vortex ring descended, it entrained fluid from the moving surface layer and carried this fluid downward. Reynolds reported that the nonmoving fluid from below would rise up and replace the surface fluid, diminishing the motion of the surface which is essential to the continuity of the wave.

Later, Ashton and O'Sullivan (1949), Barnaby (1949), and Sainsbury and Cheeseman (1950) further investigated Reynolds' theory. Each of these groups conducted experiments involving drops of dye striking a water surface. Their conclusions were inconclusive in testing Reynolds' theory. Although vortex rings were observed in all experiments, the rings' effect on wave attenuation was not clearly established.

The interaction of water drops on surface waves was explored subsequently by Siscoe and Levin (1971). They found two very different processes, depending upon the raindrop's point of incidence on the wave: a reflection process and an absorption process. In an absorption event, the drop strikes at or near the wave crest and TKE is in-

corporated into the wave field. A reflection event occurs in the event of rain striking the trough, and the TKE of the drop goes into producing subsurface turbulent mixing. They found that during an absorption event the energy supplied by an impacting drop amplified the surface wave field which propagated out from the point of impact. Drops were colored by dye to investigate further wave formation and subsurface interaction. The dye did not penetrate the surface for an absorption event, while during reflection events, dye penetrated to the subsurface waters due to drop-induced mixing. The observed motions of the dye that accounted for this mass transfer were vortex rings and weakly defined circulation cells that reached a depth of 5-10 cm with an occasional ring penetrating deeper.

2. Characteristics of Vortex Rings

When raindrops strike the sea surface a portion of their energy is transferred into the water column in the form of vortex rings. Keedy (1967) conducted an extensive study on the formation of vortex rings by free surface interactions. He allowed water drops of various radii to fall from heights of 2.5 inches or less, and he observed ring formation and penetration. Keedy found that vortex rings penetrate to a maximum depth of approximately 10 cm. Also noted were density differences between the drop and the base solution which were important in determining the maximum penetration depth of the vortex ring. For a drop with a density lower than the density of the base solution, the vortex ring expanded in diameter more rapidly than if both drop and base solutions were of the same density.

Maxworthy (1972) observed the propagation of vortex rings produced using a membrane apparatus in an experimental tank. He found that as the rings traveled they continuously entrained surrounding fluid and grew in volume. At the same time, the rings were losing vorticity into a wake and decreasing in velocity. Maxworthy also observed two different processes when two similar rings, one ahead of the other, came into

contact. If both rings had the same velocity, the rearward one would distort and squeeze into the forward ring through the rear wake area. The rearward ring was then wrapped around the inner part of the forward ring to form a single larger vortex. If the velocity of the rearward ring was larger than that of the forward ring, the rearward ring's entry into the forward ring caused the combined ring to oscillate longitudinally. If the trailing ring's velocity is much greater than that of the front ring Maxworthy found that the newly formed ring would disintegrate with a faster ring propagating ahead of a slower moving ring.

Batchelor (1967) had previously found a similar occurrence involving two similar vortex rings and suggested an interaction analogous to " leap frog. " The velocity field of the rear ring has a radially outward component at the position of the forward ring. As the radius of the front ring increases, travel speed decreases. At the same time, the rearward ring undergoes a relative increase in speed and passes through the larger vortex, becoming the lead ring. This maneuver is then repeated. The interaction of these rings suggests that random rings produced in nature will collide, changing the ring's characteristics and velocity. The gross effect will be to reduce the penetration depth expected from a single vortex ring.

3. Rain-induced Mixed Layer Changes

Rather than study individual drops and vortex rings, Green and Houk (1979) studied populations of raindrops and the subsequent mixed layer formation. Observations of changes to the mixed layer depth (MLD) were made by determining the location of the thermocline. This circumvented the need to consider individual vortices in favor of an integrated turbulent mixed layer. Green and Houk found that a mixed layer had developed after 20 minutes of rain, with a deeper MLD associated with the larger drop sizes. The depth of the mixed layer in salt water was approximately one third that of freshwater due to the larger downward buoyancy flux. All other parameters were held

constant. Green and Houk determined that the majority of the mechanical energy flux went directly into subsurface turbulence. The overall effect was a deepening of the MLD as the energy from raindrops diffused down into the water column, deepening the MLD 10-30 cm in freshwater and 5 to 10 cm in saltwater.

4. Manton's Analytical Approach

Manton (1973) presented an analytical approach to explain rain-induced vortex ring mixing and the resulting wave attenuation. Through a scale analysis, using the raindrop's terminal velocity (V) and the horizontal wind speed (U), Manton defined a vertical and horizontal eddy viscosity:

$$\nu_v = f^{\frac{1}{2}} V l \tag{2.1}$$

$$\nu_h = f^{\frac{1}{2}} U l \tag{2.2}$$

where f represents the volume fraction of drops in the air; and l represents the turbulent length scale determined by the average distance between drops in the air. In order to use vertical and horizontal eddy viscosities in the momentum equations, Manton needed to prove that equations 2.1 and 2.2 were independent of depth. Through analytical means he proved that the shear layer thickness for a wave, on the order $\left(\frac{\nu_v}{\omega}\right)^{\frac{1}{2}}$, was smaller than the penetration depth of vortices (10-20 cm). Erroneously, the shear layer thickness is the depth associated with friction from a boundary and not the depth associated with the wave energy, 1 k. By assuming that the maximum mixing depth is related to vortex ring penetration, mixing should only occur at a depth of 10 to 20 cm, which is much shallower than the depth associated with the wave energy. Manton solved the linearized momentum equations using a potential velocity solution, implicitly assuming irrotational flow. However, when mixing is present the flow becomes rotational. It is still possible to predict the viscous decay of the waves by assuming that the mixing is

uniform over depth (Lighthill, 1978). If ν_v and ν_h are assumed to be equal, Manton's results would agree with such theory; however, Manton used separate values of ν_v and ν_h to incorporate the influence of wind into his solution. This is an inappropriate use of the viscous decay terms in the momentum equations. For a vortex ring, the horizontal and vertical mixing scales are of the same order, thus ν_v and ν_h should be replaced by a single eddy viscosity coefficient, ν , for the mixed layer. Wind, which is not considered in this study, is normally introduced as an additional surface stress source term in the momentum equations and does not appear as part of the viscous dissipation term. Thus there are two serious objections to Manton's effort:

1. introducing mixing over the entire water column, and
2. incorporating the influence of wind into ν.

This study uses a numerical solution of the Navier-Stokes equations for a surface gravity wave. A single viscous coefficient ν will be applied to a thin " mixed layer " and the resulting attenuation will be estimated and compared to classical theory (Lighthill, 1978).

III. METHODS

A. THE MODEL

A numerical model, SOLA-VOF (Nichols et al, 1980), developed at the Los Alamos National Laboratory in New Mexico was used for this study. This model is a general two-dimensional finite differencing Eulerian code which allows for complicated computational domains with variable boundary conditions, free surface shapes, variable surface tension and compressibility. Behavior of the fluid is determined by solving the Navier-Stokes equations:

$$\frac{\partial u}{\partial t} + u\frac{\partial u}{\partial x} + v\frac{\partial u}{\partial y} = -\frac{1}{\rho}\frac{\partial p}{\partial x} + \nu\left[\frac{\partial^2 u}{\partial x^2} + \frac{\partial^2 u}{\partial y^2}\right] \tag{3.1}$$

$$\frac{\partial v}{\partial t} + u\frac{\partial v}{\partial x} + v\frac{\partial v}{\partial y} = -\frac{1}{\rho}\frac{\partial p}{\partial y} + g + \nu\left[\frac{\partial^2 v}{\partial x^2} + \frac{\partial^2 v}{\partial y^2}\right] \tag{3.2}$$

where u is the horizontal velocity, v is the vertical velocity, g is the body acceleration due to gravity, ν is the coefficient of kinematic viscosity, and ρ is the fluid density. In addition to the momentum equations the incompressible mass conservation equation:

$$\frac{\partial u}{\partial x} + \frac{\partial v}{\partial y} = 0 \tag{3.3}$$

must be satisfied at each time step. To advance a solution through a one time increment the model must go through the following three steps:

1. Explicit approximations of Eq. (3-1) and Eq. (3-2) are used to compute the first guess for the new time-level velocities using the initial conditions or the previous time-level values for all advective, pressure, and viscous accelerations.
2. To satisfy the continuity equation, Eq. (3-3), pressures are iteratively adjusted in each cell and the velocity changes induced by each pressure change are added to

the velocities computed in step (1). A repetitive process is required because the change in pressure needed in one cell to satisfy Eq. (3-3) will upset the balance in the four adjacent cells.

3. The cell fluid function defining fluid regions is then updated to give the new fluid configuration.

In this manner the fluid solution can be advanced through all desired time intervals. Horizontal and vertical velocity (u,v), pressure (P), and fractional volume of fluid in a cell (F) are calculated at each time step at the cell positions shown in Fig. 2.

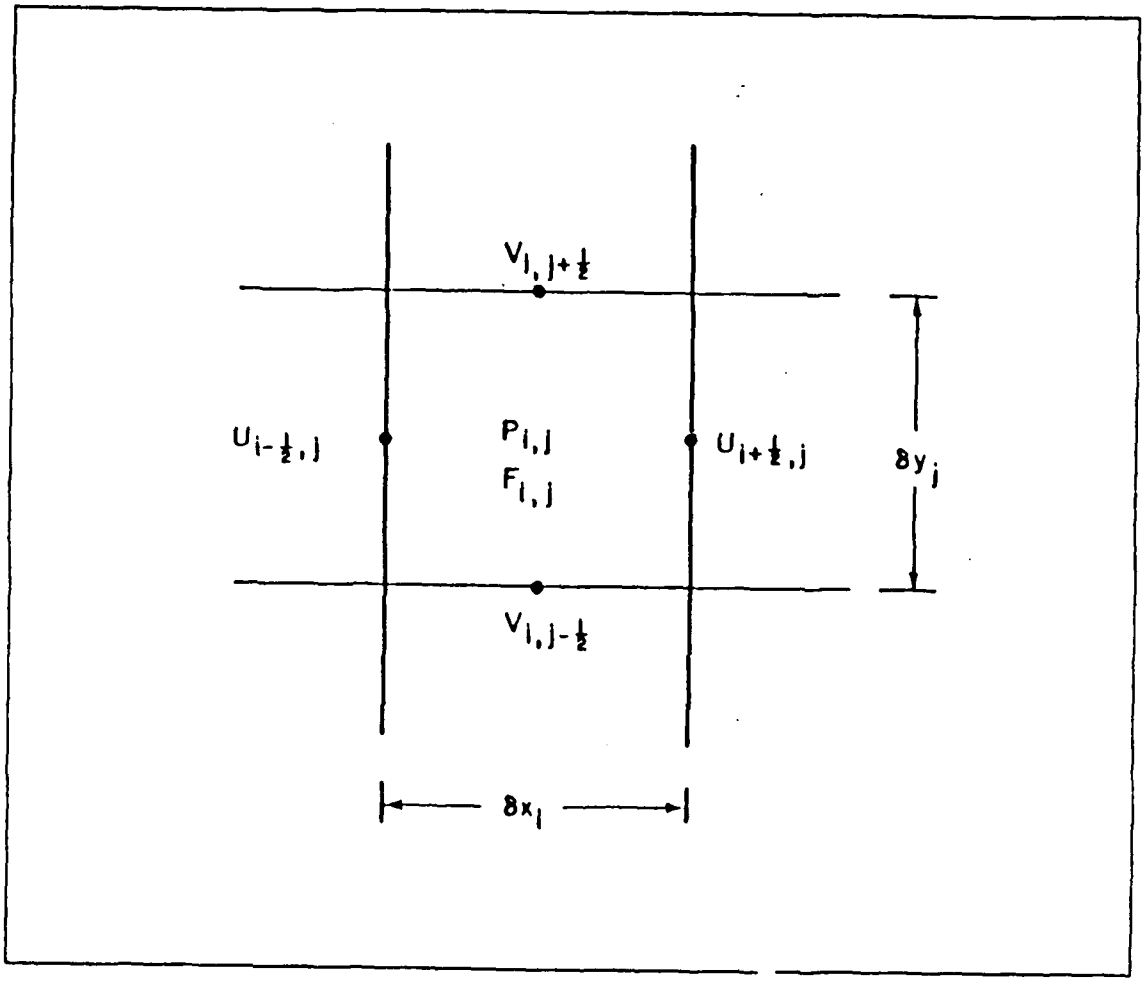

Figure 2. Typical cell configuration: U and V velocities are found on the sides and top of the cell with pressure and fluid percentage of each cell found in the center of the cell.

The fractional volume of fluid function (F) is used to identify grid cells that contain fluid, and to delineate surface, interior or boundary cells. A free surface cell is defined as a cell containing a nonzero value for F and having at least one neighboring cell that contain a zero value for F. Cells with nonzero F values and no empty neighbors are treated as cells full of fluid.

Introduction of variable viscosity into the code required a change to the code. This was accomplished by: (1) establishing a viscosity grid and (2) encoding this viscosity grid into the viscous terms. The viscosity grid was established by identifying three areas, v_1, the mixing layer at the surface of the wave, v_2, a transition zone from the mixed layer to the turbulent free layer defined as $\frac{v_1 + v_3}{2}$ and v_3, the base layer, (effected by molecular viscosity only). The turbulent mixing layer was defined as those cells which were between the free surface and the desired mixing depth. An example is given in Fig. 3 depicting the mixing layer following the surface. The height change is from the numerical initialization of the wave.

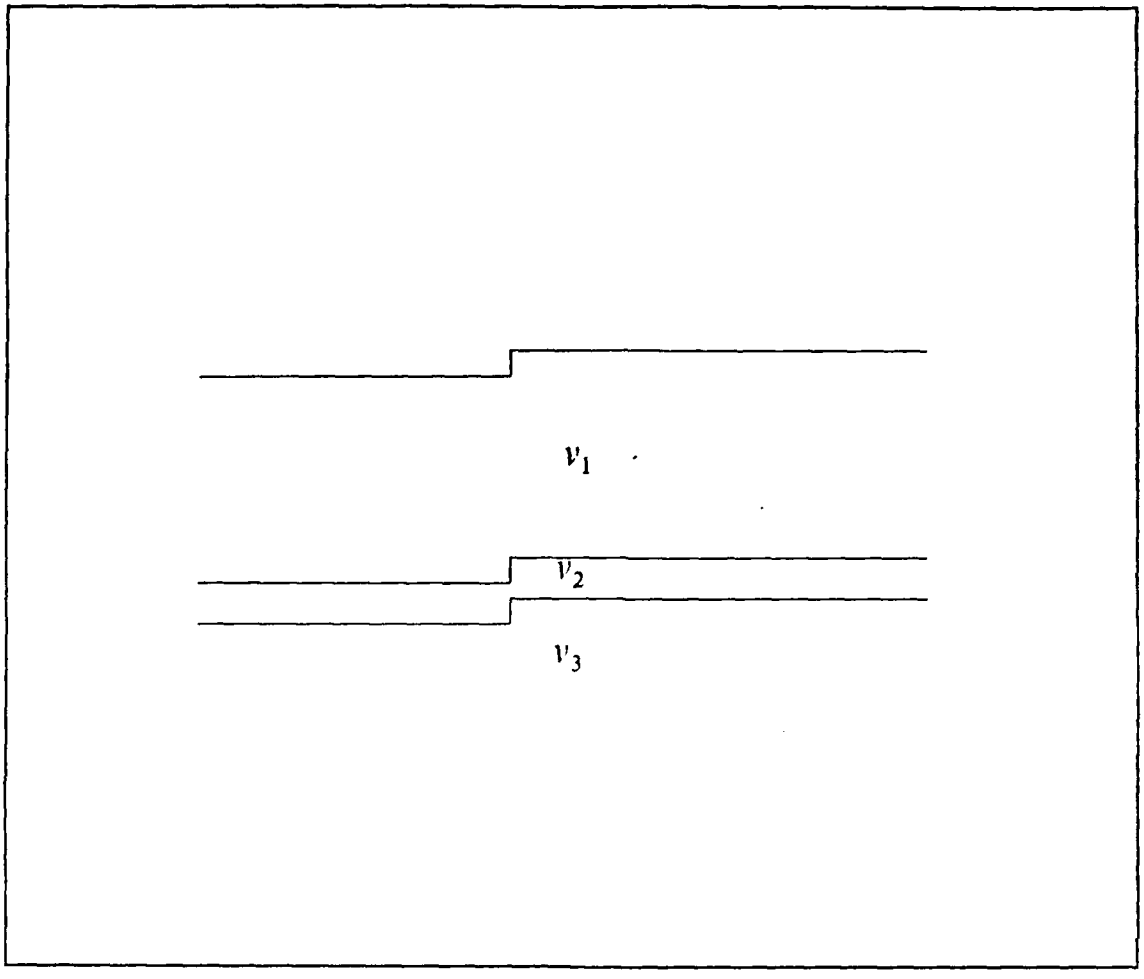

Figure 3. Kinematic viscosity grid configuration: The setup of the viscosity grid where ν_1 is the surface mixing layer, ν_2, the transition layer, and ν_3 the base fluid layer.

The viscosity grid was redefined at each time step resulting in a moving mixing layer having a constant thickness. A four corner average was then used to obtain a value of ν for each computational cell. The single derivative form of the momentum equations (Harlow 1980):

$$\frac{du}{dt} = -\frac{1}{\rho}\frac{\partial p}{\partial x} + \frac{\partial}{\partial x}\left[2\nu\frac{\partial u}{\partial x}\right] + \frac{\partial}{\partial y}\left[\nu\left(\frac{\partial u}{\partial y} + \frac{\partial v}{\partial x}\right)\right] \qquad (3.4)$$

$$\frac{dv}{dt} = g - \frac{1}{\rho}\frac{\partial p}{\partial y} + \frac{\partial}{\partial y}\left[2\nu\frac{\partial v}{\partial y}\right] + \frac{\partial}{\partial x}\left[\nu\left(\frac{\partial u}{\partial y} + \frac{\partial v}{\partial x}\right)\right] \qquad (3.5)$$

was used to reduce numerical noise associated with calculating second derivatives at the boundary of the two layers.

B. THE WAVE

This study focused on the attenuation of deep water waves resulting from rain-induced mixing. To simulate this a computational domain was initialized representing a fluid vessel or tank 1.4 m wide and 3.0 m deep. A Mean Fluid Height (MFH) of 2.8 m was selected. The tank depth of one wavelength was chosen to ensure that bottom effects would be negligible during the propagation of the wave. According to deep water wave theory, velocity at the base of the tank is smaller than the surface velocities by a factor of $e^{-kz} = e^{-2\pi} \ll 1$. Furthermore, a small amplitude wave (3 and 6 cm) was chosen to maintain stability of the wave. During the early part of the project the wave was found to break if the amplitude became greater than 10 cm due to the manner in which the code assigned velocities at the free surface. Normally a surface velocity is set to be the same value as the nearest horizontal neighbor cell. Depending on the direction of wave propagation this horizontal movement of velocities occasionally produced an unrealistic velocity discontinuity in the vertical. This problem was corrected by making the nearest neighbor cell directly below the surface cell.

A 2.8 m wavelength standing wave was chosen to minimize continuation boundary problems associated with a progressive wave, and to facilitate a simple initial condition having no velocities. A standing wave is actually two progressive waves propagating in opposite directions given by: $\eta = \eta_0 \cos kx \cos \omega t$ where η_0 is the wave amplitude, k is the wave number, and ω is the radial frequency. A progressive wave was simulated by initializing one-half wavelength of the standing wave using the instantaneous wave height: $\eta = MFH - \eta_0 \cos kx$ at t = 0 for a domain of $0 < x < \frac{\lambda}{2}$. The waves initial configuration is seen in Fig. 4 under steady state conditions. Velocity vectors are also plotted for the initial steady state condition and are represented by a vector of zero length.

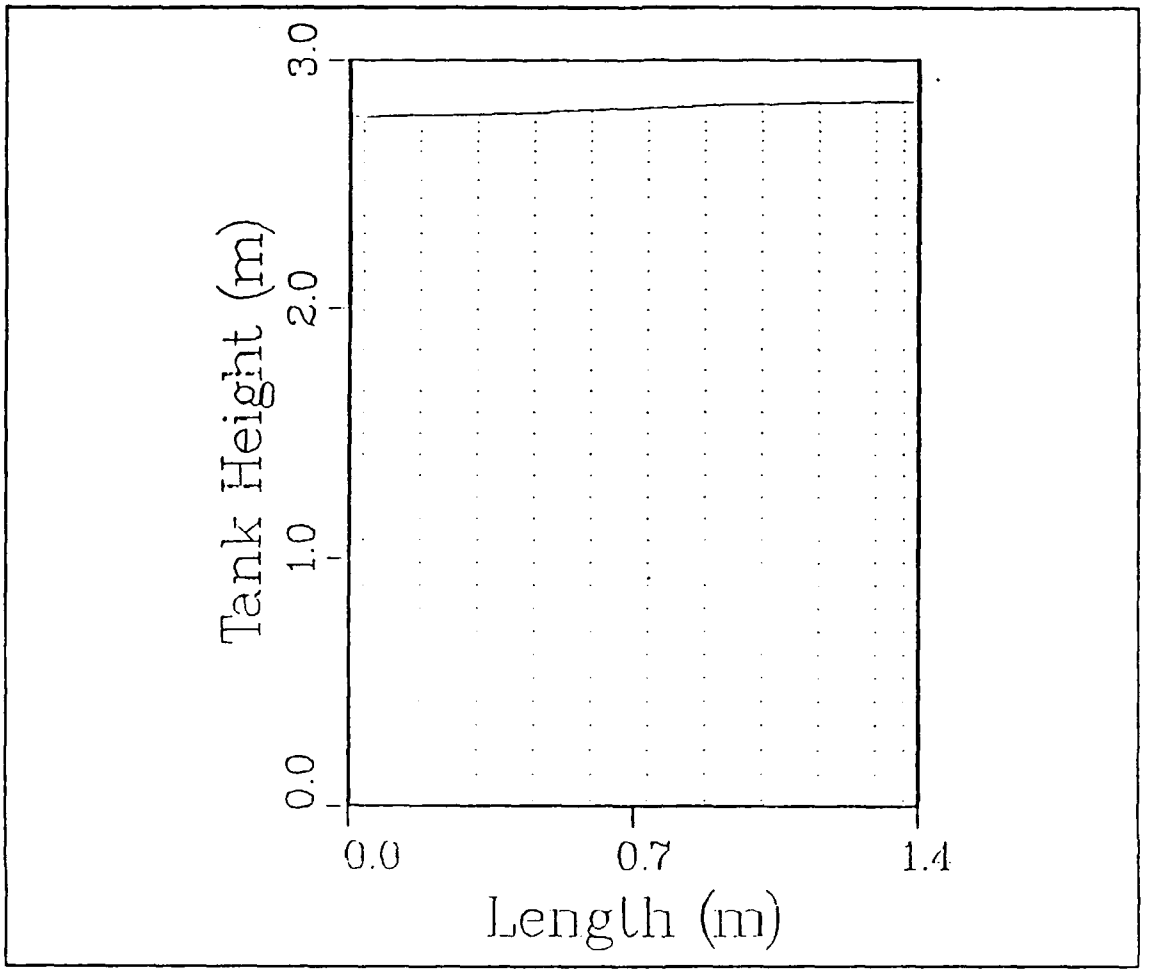

Figure 4. Initial wave configuration for all experiments: The one-half wavelength at rest prior to being released.

The wave was released from rest and observed as it propagated through the tank. Wave dynamics were reviewed and compared to theoretical values to ensure that the wave and code had been properly developed.

Validation of the wave was accomplished by examining the period, the vertical U velocity profile, the potential and kinetic energy, and the attenuation characteristics of the wave. According to deep water wave theory a period of 1.34 s is derived. In Fig. 5 and Fig. 6 the wave is seen to take approximately 1.3 s to propagate from a maximum amplitude at the right wall to the left and back to the right wall coinciding with theory.

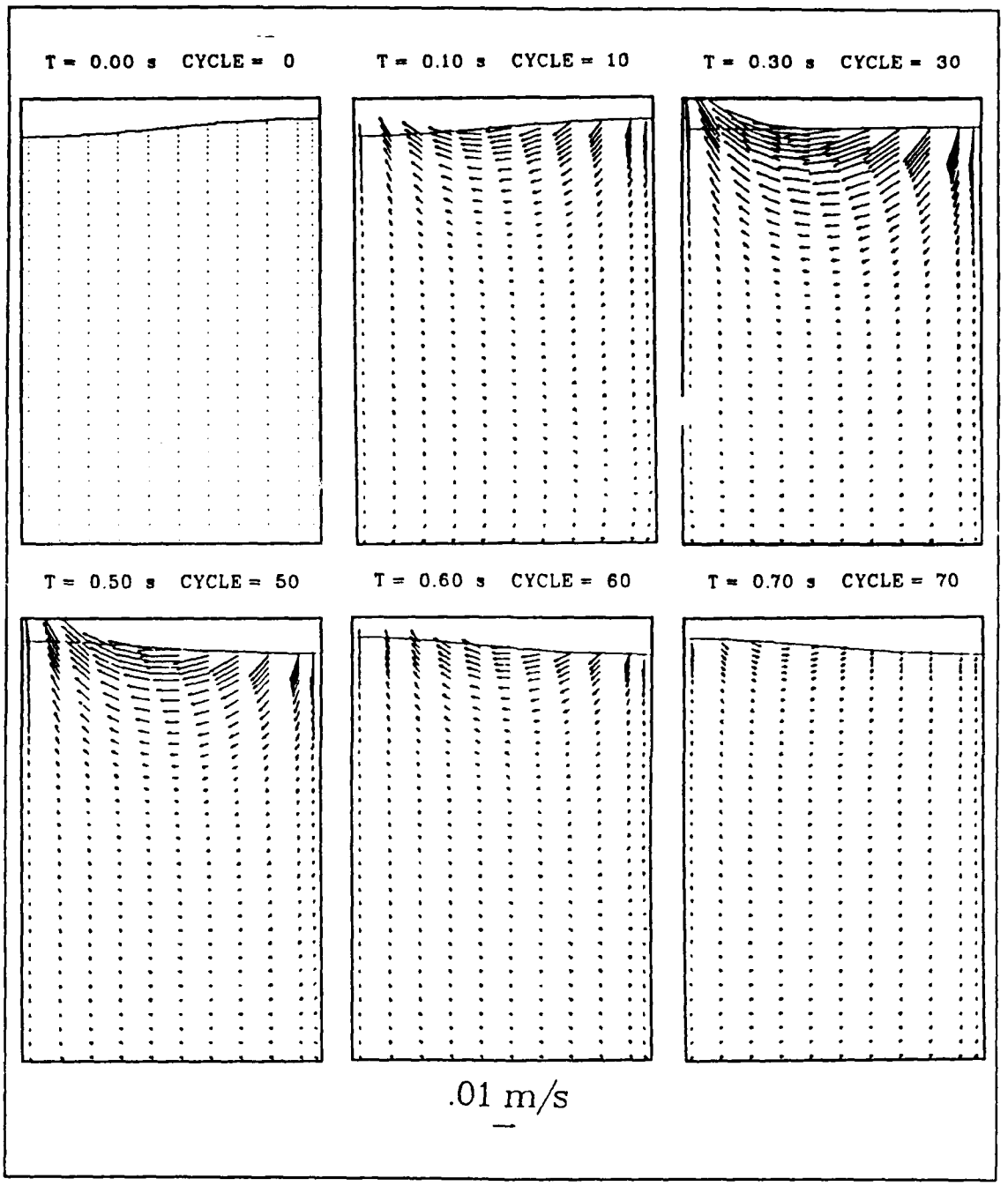

Figure 5. Wave propagation through the tank: The wave is observed propagating from rest toward the left wall of the tank.

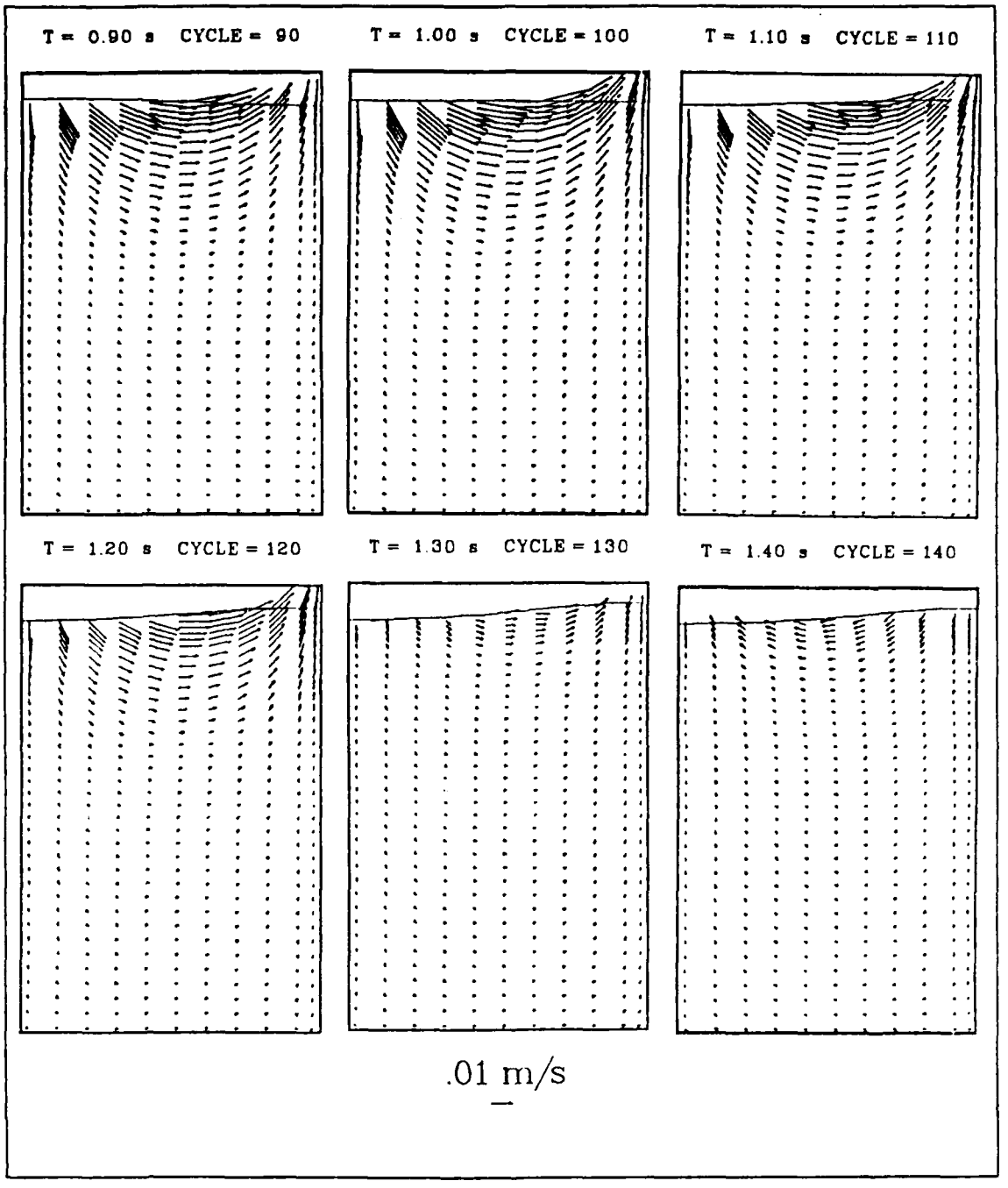

Figure 6. Wave propagation: The wave is now propagating toward the right wall of the tank.

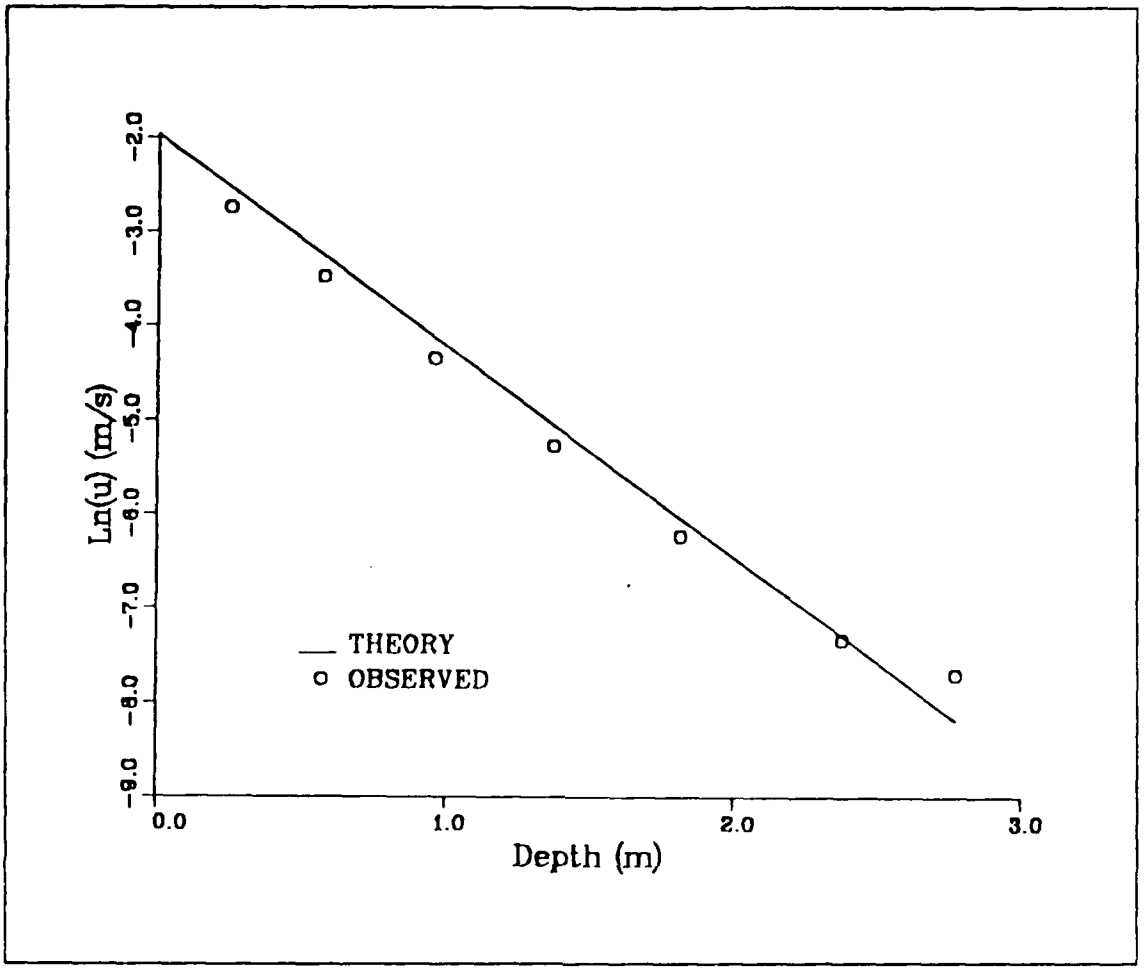

Figure 7. Natural log of u vs depth.

To validate the velocity field a vertical U velocity profile was examined and compared to theory: $u = u_0 e^{-kz}$. The theoretical velocity decay profile was derived and plotted, Fig. 7. The numerical profile was consistent with theory except for an inconsistency seen near the bottom of the tank which may be due to numerical noise contamination.

The energy of a standing wave is known to be periodic alternating from Potential Energy (PE) to Kinetic Energy (KE) over time. Theoretical values of the total energy density are obtained by adding the energy density of the two progressive waves, ($\frac{1}{2} \rho g \eta_r^2 \lambda$) each with half the amplitude, ($\eta_r = \frac{1}{2} \eta_0$) of the standing wave. For a wave amplitude of, η_0, 6 cm the total energy is $\frac{1}{4}\rho g \eta_0^2 = 12.348$ J and for a 3 cm amplitude, 3.087 J. To compute energy numerically, PE density was calculated from:

$$PE = \tfrac{1}{2}\,\rho\, g\, \eta^2\, dx\, dz \tag{3.6}$$

by summing over the surface of the wave, where η is found to be the distance the wave surface is above or below the MFH. KE density was found by summing:

$$KE = \tfrac{1}{2}\,\rho\, V^2\, dx\, dy\, dz \tag{3.7}$$

over the domain of the tank where $V^2 = (u^2 + v^2)$ for each cell. The energy for a 6 cm amplitude wave propagating under normal conditions of molecular viscosity ($\nu = 10^{-6}\, m^2\, s^{-1}$) is seen in Fig. 8. The peak energy values are consistent with theory. Initially PE is a maximum and KE is zero. As the wave propagates PE approaches zero and KE reaches a maximum at each one-quarter cycle. PE becomes a maximum at each one-half cycle as KE approaches zero.

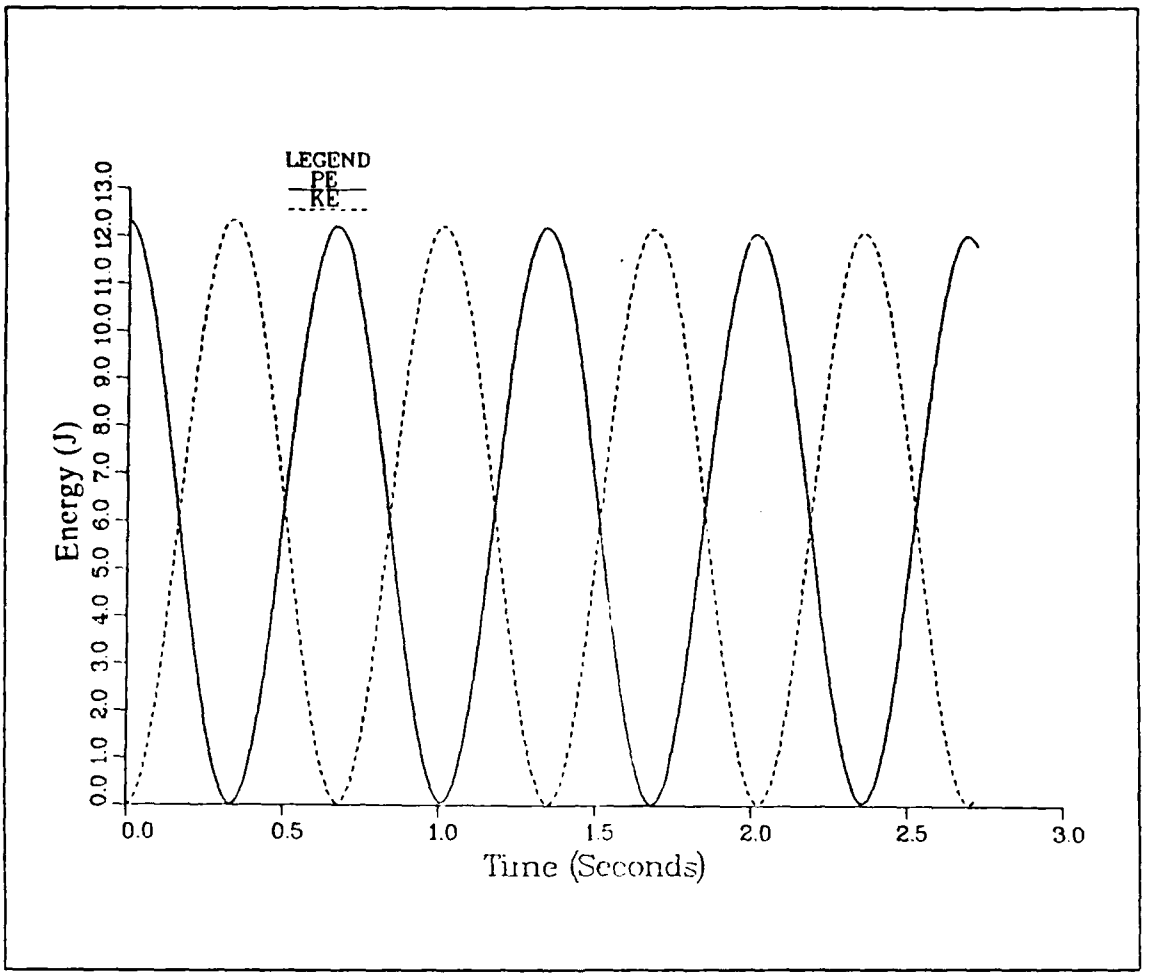

Figure 8. Potential and Kinetic energy vs time: The sinusoidal nature of PE and KE is depicted for the wave as it propagates over time, $\nu = 10^{-6}\ m^2\ s^{-1}$.

Kinematic viscosity was used to represent the turbulent mixing occurring in the water column. The values used ranged from $10^{-6}\ m^2\ s^{-1}$ representing molecular effects to $10^{-2}\ m^2\ s^{-1}$ representing high turbulent conditions. This range included values found by Manton: $3 \times 10^{-4}\ m^2\ s^{-1}$ for a light rain event and $1.6 \times 10^{-3}\ m^2\ s^{-1}$ for a heavy rain event. This range also included Green and Houk's estimate for the mixed layer eddy viscosity coefficient, $5 \times 10^{-3}\ m^2\ s^{-1}$. The kinematic viscosity was kept constant over the entire water column to determine if attenuation effects were following theory. Both amplitudes were used for this test. Two different methods were used to determine the rate of energy change over time. The slope of the decay of peak kinetic energy was used

as a direct representation of the rate of energy change. From Fig. 9 the attenuation due to $\nu = 10^{-2}\ m^2\ s^{-1}$ gives a normalized slope of 0.15 which is nearly consistent with theory, $4\nu k^2 = 0.2$. A more accurate method was found using the internal dissipation function (Schlichting, 1960):

$$\Phi = 2\left[\left(\frac{\partial u}{\partial x}\right)^2 + \left(\frac{\partial u}{\partial y}\right)^2\right] + \left(\frac{\partial u}{\partial y} + \frac{\partial v}{\partial x}\right)^2 \tag{3.8}$$

This represents the decrease of energy from viscous effects and does not include the redistribution of energy into the wave. At each time step the change of energy was calculated and normalized by the instantaneous kinetic energy. Final processing of the data was then conducted by taking the average of the rate of change of energy divided by KE, i.e., Φ/KE, for $KE > 1$. This was required due to an erroneous spike developing as KE became less than one, as seen in Fig. 10. This was done for both the 3 and 6 cm amplitude cases, the results of which are given in Tables 1 and 2, showing good agreement with theory.

Table 1. RESULTS FOR A 3 CM AMPLITUDE WAVE.

Nu $m^2\ s^{-1}$	Φ/KE	Theory $8\nu k^2$
1.E-6	.0000394	.000040
1.E-4	.00394	.0040
3.E-4	.0118	.0120
1.E-3	.0393	.0400
1.6E-3	.0626	.0640
1.E-2	.380	.400

Table 2. RESULTS FOR A 6 CM AMPLITUDE WAVE.

Nu $m^2\ s^{-1}$	Φ/KE	Theory $8\nu k^2$
1.E-6	.000039	.000040
1.E-4	.00397	.0040
3.E-4	.0118	.0120
1.E-3	.0395	.0400
1.6E-3	.0627	.0640
1.E-2	.384	.400

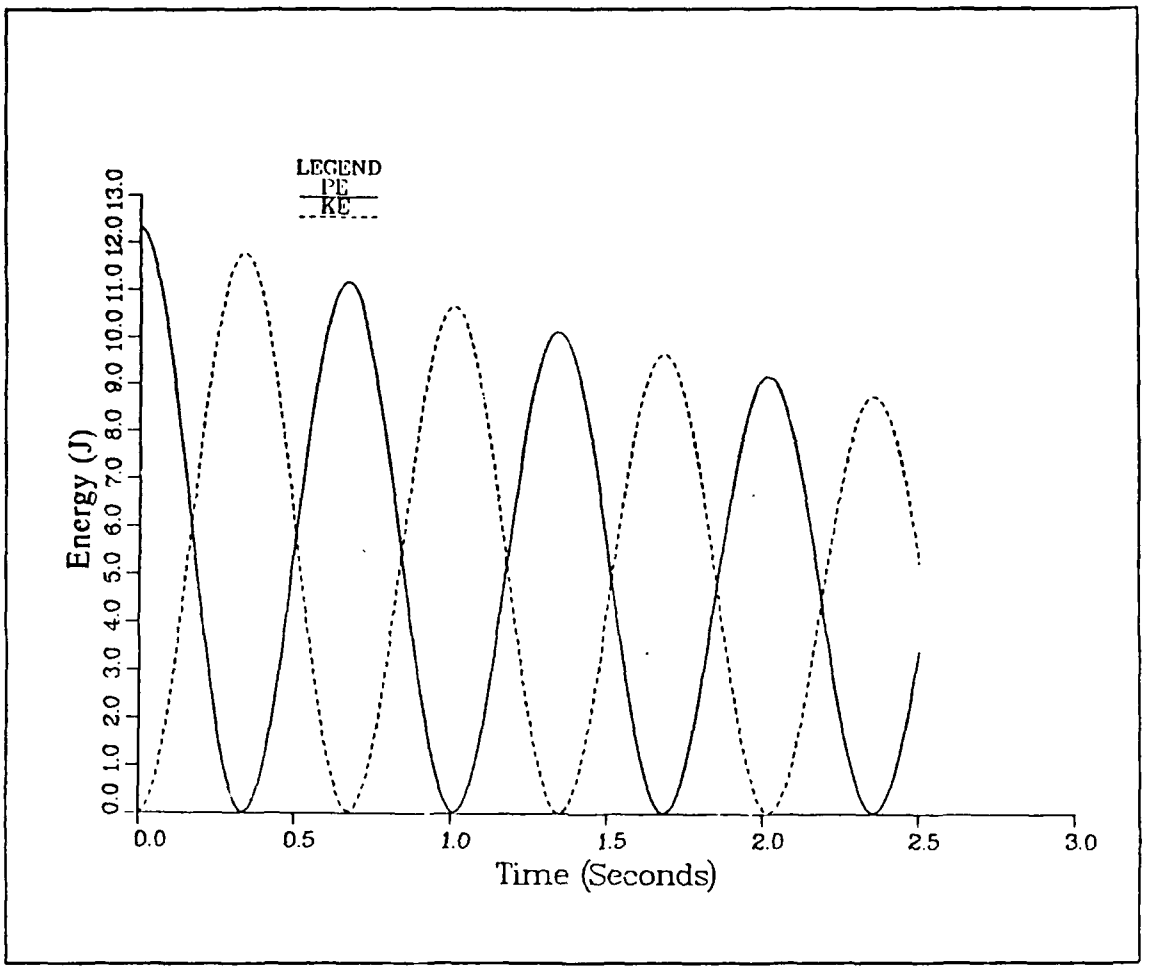

Figure 9. Potential and Kinetic energy vs time: The sinusoidal nature of PE and KE are depicted for the wave as it propagates over time, $\nu = 10^{-2}\, m^2\, s^{-1}$.

C. THE MIXED LAYER PROBLEM

Due to observations by Keedy, Siscoe and Levin, and Houk and Green two mixing depths, 10 and 20 cm were used in this study. The 10 cm depth was representative of the maximum penetration depth of vortex rings formed by raindrops striking the ocean surface while 20 cm represented an increased mixing depth penetration, but occurring more infrequently. Kinematic viscosity of the base layer was set at $10^{-6}\, m^2\, s^{-1}$. The surface mixing layer was varied from 10^{-4} to $10^{-2}\, m^2\, s^{-1}$. As for the single layer case, Φ/KE was calculated at each time step and averaged for all values of KE greater than

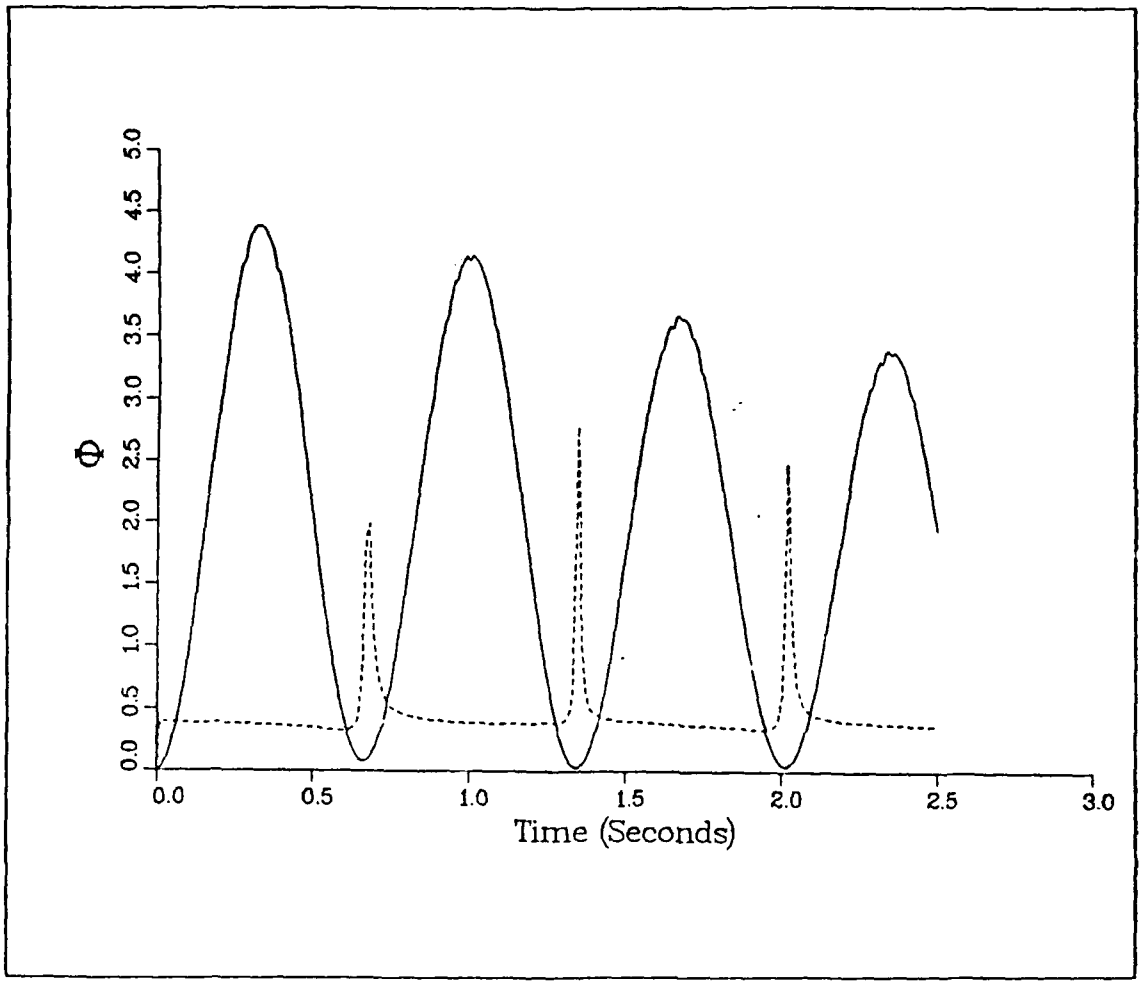

Figure 10. Rate of energy change: Attenuation for Φ (—) and Φ/KE (---) with $\nu = 10^{-2}\, m^2\, s^{-1}$.

one. These results were compared to the expected theoretical values of the two layers. The theoretical values shown are $\frac{\nu_1}{\nu_3}$ where ν_1 is the mixing if the viscosity coefficient in the mixed layer is used and ν_3 is the mixing if the viscosity coefficient (molecular) of the lower layer is used.

The effects of increasing ν in the top 10 cm layer is expected to increase attenuation, although less than expected if the entire water column is more turbulent. Doubling the mixing layer to 20 cm is hypothesized to double the attenuation seen in the 10 cm surface layer case. By increasing the penetration depth more kinetic energy should be taken out of the wave, i.e.,dampen the wave.

The results shown in Tables 3 and 4 are for a 10 cm mixed layer and in Table 5 for a 20 cm mixed layer.

Table 3. RESULTS FOR A 3 CM AMPLITUDE WAVE, 10 CM MIXING DEPTH.

Nu	Φ/KE	Theory $8\nu k^2$ ν_1/ν_3
1.E-4	.00162	.0040 .00004
3.E-4	.00477	.0120 .00004
1.E-3	.0157	.0400 .00004
1.6E-3	.0243	.0640 .00004
1.E-2	.1269	.4000 .00004

Table 4. RESULTS FOR A 6 CM AMPLITUDE WAVE, 10 CM MIXING DEPTH.

Nu	Φ/KE	Theory $8\nu k^2$ ν_1/ν_3
1.E-4	.00165	.0040 .00004
3.E-4	.00489	.0120 .00004
1.E-3	.0159	.0400 .00004
1.6E-3	.0252	.0640 .00004
1.E-2	.1379	.4000 .00004

Table 5. RESULTS FOR A 6 CM AMPLITUDE WAVE, 20 CM MIXING DEPTH.

Nu	Φ/KE	Theory $8\nu k^2$ ν_1/ν_3
1.E-4	.00259	.0040 .00004
3.E-4	.00773	.0120 .00004
1.E-3	.0256	.0400 .00004
1.6E-3	.0409	.0640 .00004
1.E-2	.2440	.4000 .00004

1. Single Layer Wave

Using molecular mixing, $\nu = 10^{-6}\ m^2\ s^{-1}$, (Tables 1 and 2) a 3 cm amplitude wave required 46,000 wave periods and a 6 cm amplitude wave required 82,000 wave periods to reduce KE to an arbitrary cutoff value of 0.5 N-m. By comparison, the rate of energy change for a 3 cm amplitude wave with a 10 cm mixed layer ($\nu_1 = 10^{-2}\ m^2\ s^{-1}$) showed a

3,000 fold increase in the rate of energy loss, requiring only 14 wave periods to dampen the wave. An almost identical rate of energy loss is seen for the 6 cm amplitude wave with dampening occurring in 22 wave periods. If the mixing depth was doubled to 20 cm there was a 6,200 fold increase in the rate of energy change which is nearly double that of the 6 cm amplitude wave with a 10 cm mixing depth. Thus by increasing turbulent mixing in a thin surface layer an increase in the rate of energy change (3000-6000 fold or greater) can be produced. This is especially noteworthy for short gravity and capillary waves whose energy is mostly contained within the mixing layer.

2. Rain's Effects on Waves

a. 10 cm Mixing Depth

To model the effects of rain, three viscosities were directly associated with rain events:

1. $3.0 \times 10^{-4}\ m^2\ s^{-1}$ for a light rain event (5 *mm/hr* rain rate) (Manton)
2. $1.6 \times 10^{-3}\ m^2\ s^{-1}$ for a heavy rain event (12 *mm/hr* rain rate) (Manton)
3. $5.0 \times 10^{-5}\ m^2\ s^{-1}$ for a heavy rain event (14 *mm/hr* rain rate) (Green and Houk)

Viscosities (1) and (2) were used in this study. Comparing the results for these two viscosities showed that as the rain rate and the turbulent mixing increased, an increase in the attenuation of the wave also occurred. The time interval required to dampen a 3 cm amplitude wave with 10 cm mixing depth was 380 wave periods for light rain and 80 wave periods for heavy rain. Doubling this wave amplitude and maintaining a constant 10 cm mixing depth, is found to increase the wave periods required to dampen the wave. During a light rain event the wave is dampened within 655 wave periods and 126 wave periods during a heavy rain.

b. 20 cm Mixing Depth

As shown in Table 5, doubling the mixing depth did not double the rate of energy change as hypothesized, although a significant (50-80%) change did occur. For a wave of 2.8 m wavelength and 6 cm amplitude, a light rain event caused the wave to be dampened within 420 wave periods and within 80 wave periods for a heavy rain event. This is a reduction of approximately 38% of the wave periods required to dampen the same wave with a 10 cm mixing depth.

IV. CONCLUSION

Strong rain-induced mixing within a very thin surface layer will increase the attenuation rate of surface gravity waves by several orders of magnitude over the rate of attenuation due to molecular viscosity alone. In this case study a single wavelength (2.8m) was used together with two mixed layer depths (10 and 20 cm). In the case of strong mixing ($\nu = 10^{-2}\, m^2\, s^{-1}$) with a 10 cm thick mixed layer, the wave was dampened with 12-24 wave periods compared to 46,000 wave periods for molecular viscosity alone. Using estimates of the eddy mixing coefficients for heavy and light rain from Manton ($\nu = 1.6x10^{-3}\, m^2\, s^{-1}$ and $\nu = 3x10^{-4} m^2 s^{-1}$) , the wave is still dampened within 126 and 655 wave periods, respectively. Increasing the mixed layer depth to 20 cm produced a significant increase in attenuation, reducing the nunber of wave periods required to dampen the wave to 80 and 420 wave periods, respectively for heavy and and light rain. This influence of rain on wave attenuation has several potential applications.

Scatterometer and SAR observations of the sea surface depend on the presence of short gravity and capillary waves. These waves are generally shorter than the case study wavelength (2.8 m) and they will be even more strongly attenuated by rain-induced mixed layers. Thus, this theory can be used to explain the observed SAR imagery in rainy regions (dark image) and may allow a correction to be applied to scatterometer algorithms used to measure wind speed from small scale ocean roughness. This should increase the accuracy of weather forecasts for marine shipping. The damping of slightly longer gravity waves present in ship wakes is also of interest. Rain will attenuate these waves and thus mask the ship's wake, decreasing the chance of detection by other remote sensing techiques. Rainfall measurements can also be incorporated into wave and surf forecasts as wave length dependent attenuation. This should increase the accuracy of such models by decreasing the energy contained in the high frequency spectrum.

This study has developed a boundary layer that resembles the shape of the water surface which may assist in simulating mixing problems more realistically. The effect of turbulent kinetic energy could be introduced numerically by using the turbulent kinetic energy equation. This equation would provide a "Reynolds' eddy viscosity coefficient" for each cell which could then be used directly rather than by defining an arbitrary mixed layer. This will allow variable surface gravity wave attenuation as the mixed

layer deepens. Through this method the effect of a finite duration rain squall on mixed layer depth and wave attenuation might be estimated.

This study focused on one wavelength, two amplitudes and two mixing depths. It is recommended that further numerical studies be conducted with larger wavelengths, higher wave amplitudes and deeper mixing depths. These factors will identify cutoff regions where rain-induced attenuation no longer has an effect on the wave. Wave tank experiments would also benefit numerical modeling to assist in parameter formations for the many inputs necessary for turbulent kinetic energy models.

REFERENCES

Ashton, E. W. S. and J. K. O'Sullivan, 1949: Effect of Rain in Calming the Sea, *Nature*, **164,** 320.

Barnaby, C. F., 1949: Effect of Rain in Calming the Sea, *Nature*, **164,** 968.

Batchelor G. K. 1967: *An introduction to fluid dynamics*, Cambridge University Press, 615 pp.

Caldwell, D. R. and W. P. Elliot, 1971: Surface stresses produced by rainfall. *J. Phys. Oceanogr.*, **1**, 145.

Fu, L. and B. Holt 1982: Seasat views oceans and sea ice with synthetic-aperture radar. JPL Publication 81-120, 200 pp.

Garwood, R. W., 1989: Unpublished manuscript.

Green, T. and D. F. Houk, 1979: The mixing of rain with near-surface water. *J. Fluid Mech.*, **90,** 569.

Keedy, H. F., 1967: Vortex rings formed by free surface interaction. Ph.D. Dissertation, The University of Michigan, 141 pp.

Lighthill, J. M., 1978: *Waves in Fluids*, Cambridge University Press, 504 pp.

Livezey, M. S., 1988: Discrete precipitation effects on seasonal mixed layer dynamics in the North Pacific Ocean. M.S. Thesis, Naval Postgraduate School, Monterey, CA., Sep., 71 pp.

Manton, M. J., 1973: On the Attenuation of Sea Waves by Rain. *Geophys. Fluid Dyn.*, 5, 249 - 260.

Maxworthy T., 1972: The Structure and Stability of Vortex Rings, *J. Fluid Mech.*, **51**, 15 - 32.

Nichols, B. D., C. W. Hirt, R. S. Hotchkiss, 1980: SOLA-VOF: A solution algorithm for transient fluid flow with multiple free boundaries, Los Alamos Scientific Laboratory report LA-8355, 119 pp.

Sainsbury, G. L. and I. C. Cheeseman, 1950: Effect of Rain in Calming the Sea, *Nature*, **166**, 79.

Schlichting, H., 1960: *Boundary layer theory*, McGraw-Hill, New York, 300 pp.

Thorpe, S.A. 1984: The effect of Langmuir circulation on the distribution of submerged bubbles caused by breaking wind waves, *J. Fluid Mech.*, **142**, 151.

INITIAL DISTRIBUTION LIST

		No. Copies
1.	Defense Technical Information Center Cameron Station Alexandria, VA 22304-6145	2
2.	Library, Code 0142 Naval Postgraduate School Monterey, CA 93943-5002	2
3.	Chairman (Code 63Rd) Department of Meteorology Naval Postgraduate School Monterey, CA 93943-5000	1
4.	Chairman (Code 68Co) Department of Oceanography Naval Postgraduate School Monterey, CA 93943-5000	1
5.	Professor R. W. Garwood (Code 68Gd) Department of Oceanography Naval Postgraduate School Monterey, CA 93943-5000	1
6.	Professor Jeffrey A. Nystuen (Code 68Ny) Department of Oceanography Naval Postgraduate School Monterey, CA 93943-5000	1
7.	Professor Chung-Shang Wu (Code 68Wu) Department of Meteorology Naval Postgraduate School Monterey, CA 93943-5000	1
8.	Lt. David W. Howell, USN NOCF Box 68 FPO Seattle, WA 98762	3
9.	Director Naval Oceanography Division Naval Observatory 34th and Massachusetts Avenue NW Washington, DC 20390	1

10. Commander Naval Oceanography Command — 1
Naval Oceanography Command
NSTL Station
Bay St. Louis, MS 39522

11. Commanding Officer — 1
Naval Oceanographic Office
NSTL Station
Bay St. Louis, MS 39522

12. Commanding Officer — 1
Fleet Numerical Oceanography Center
Monterey, CA 93943

13. Commanding Officer — 1
Naval Environmental Prediction Research Facility
Monterey, CA 93943

14. Chairman, Department of Oceanography — 1
Texas A&M University
College Station, TX 77843

15. Chief of Naval Research — 1
800 North Quincy Street
Arlington, VA 22217

16. Office of Naval Research (Code 420) — 1
Naval Ocean Research and Development Activity
800 North Quincy Street
Arlington, VA 22217